High-order elastic finite-difference modeling

Gustavo Alves and Biondo Biondi

ABSTRACT

For many years, short-offset data have been a cornerstone of reflection seismic imaging and amplitude estimation methods such as Azimuth versus Offset (AVO). However, longer offsets have increasingly become more available due to new acquisition geometries and to a greater emphasis in refraction seismic, stimulated in part by inverse methods like Full Waveform Inversion (FWI). We focus here on some of the limitations encountered in short offset versus long-offset data, specifically reflectivity estimations for higher reflection angles. We then turn our attention to a finite difference implementation of the elastic two-way wave equation, which is a necessary modeling step for truer amplitude estimation. Finally, we implement a 10^{th} order in space and 2^{nd} order in time finite-difference scheme and show a few propagation examples.

INTRODUCTION

Seismic acquisition has constantly pushed to acquire longer and longer offsets. The need to acquire longer offsets in the crossline direction, for instance, led to the development of novel streamer acquisition techniques such as wide azimuth, rich azimuth, multi-azimuth and, more recently, coil and dual coil methods (Moldoveanu et al., 2008). In most instances, these innovations were motivated by the need to illuminate a wider range of azimuths and overcome shadow zones created by complex geology (Corcoran et al., 2007), but recently, the need for longer offsets both in the inline and crossline directions has been motivated by deeper imaging targets, and the need for refraction data for traveltime tomography and FWI.

Brenders et al. (2007) analyze the impact of added offsets in wavefield tomography for the a 2D section of the 2004 BP Velocity Benchmark model. They show that tomographic velocity estimation in streamer data is limited by the maximum acquisition offset and the low frequency content in the data. In their work, a limited offset dataset (15 km) enables the recovery of the velocity model only for shallower regions. However, after incorporating offsets longer than 20 km, they show that refraction data associated to turning waves can sample deeper areas of the model, enabling the recovery of velocities at those depths.

Hilterman et al. (2000) show that, although AVO has been an important tool for identifying hydrocarbon reservoirs, some Class 1 anomalies, which are difficult to spot, could be better classified if they were treated as Class 2 anomalies identifiable

on Common Depth Point (CDP) stacks. However, the added information to make this distinction comes from longer offsets. They test the validity of this claim for offsets that are twice the target's depth. They conclude that such anomalies could be better seen in the higher offset angle stacks for a sandstone reservoir at 16,000 ft depth in the Gulf of Mexico.

Zadeh et al. (2010) show how post-critical reflections can be used to estimate velocity changes in a production environment. They use 4D data from the Valhall oilfield in the North Sea. The advantage of their methodology in comparison to traditional 4D analyses is that it can be applied to stiff rock reservoirs, such as carbonates, whereas conventional 4D encounters limitations when density varies little during production.

Skopintseva et al. (2011) focus on obtainning a better AVO result than those usually got from traditional approaches, by taking advantage of longer offset data. The group's approach to the problem involves the minimization of an objective function that compares the observed data to the reflection coefficients obtained by another methodology, presented in Aizenberg et al. (2005).

However, in order to evaluate the validity of these and other applications of long-offset data, an important first step is to be able to model both the kinematics and the amplitudes of seismic data. With that in mind, our goal is to test a finite-difference staggered-grid approach, using a high-order spatial approximation for the elastic wave equation.

In the next and following sections, we describe the limitations of traditional AVO and the methodology proposed by Skopintseva et al. (2011). Then, we show our implementation of the numerical modeling, using a finite-difference sttagered-grid velocity-stress formulation of the wave equation, based on Virieux (1986). Since our objective is to model longer offsets, which require the errors of the numerical solution to be very small even after many iterations, we replace the traditional 4^{th} order spatial approximation by a 10^{th} order spatial operator. Our claim is that this higher order will allow a more accurate solution to the wave equation and also a lower memory and computational costs due to the many model properties that need to be evaluated at each point. Finally, we show some results, obtained for a constant velocity model and a simple horizontal fluid saturated layer. Finally, we comment on some of the obstacles encountered in this methodology and the next steps in this ongoing research.

METHOD

Traditional AVO

In order to understand the limitations of current AVO analysis, we start with the physical problem that is described by the AVO equation and the linearizations involved. Figure 1 is a schematic representation of an incident plane wave on a horizontal re-

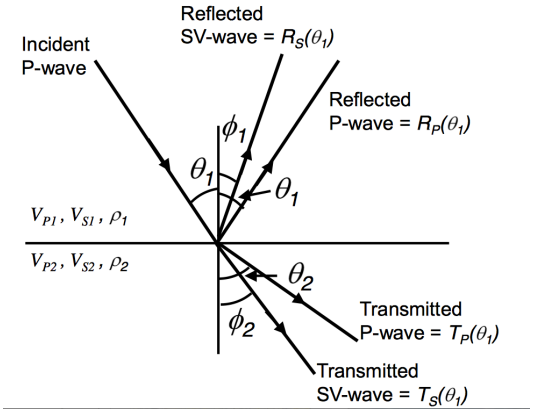

Figure 1: Schematic drawing of the incident and reflected rays for the P and S wave components on a flat reflector. The subscript 1 refers to model properties and angles in the upper region of the model, while subscript 2 refers to the new properties and angles for the lower half of the model. [**NR**]

flector and its corresponding reflected and transmited plane waves. The relationship between the reflection/transmission angles and the medium properties is described by Snell's Law. The reflectivity of these plane waves as a function of the incidence angle is described by Zoeppritz equation. The Aki and Richards (1980) approximation to Zoeppritz equation is:

$$R(\theta) = A + B\sin^2\theta + C\tan^2\theta, \tag{1}$$

where θ is the reflection angle, V_P, V_S and ρ are the pressure velocity, shear velocity and density, respectively, $A = \frac{1}{2}(\frac{\Delta V_P}{V_P} + \frac{\Delta\rho}{\rho})$, $B = -2(\frac{V_S}{V_P})^2(2\frac{\Delta V_S}{V_S} + \frac{\Delta\rho}{\rho})$ and $C = \frac{1}{2}\frac{\Delta V_P}{V_P}$. Their approximation became the starting point for modern AVO analysis. Fatti et al. (1994) further simplified their equation:

$$\begin{aligned} R(\theta) &= \frac{1}{2}\frac{\Delta I}{I}(1+\tan^2\theta) - 4(\frac{V_S}{V_P})^2(\frac{\Delta I}{I})\sin^2\theta \\ &- (\frac{1}{2}\frac{\Delta\rho}{\rho}tan^2\theta - 2(\frac{V_S}{V_P})^2(\frac{\Delta\rho}{\rho})sin^2\theta), \end{aligned} \tag{2}$$

where θ is the reflection angle, V_P and V_S are the pressure and shear velocities, respectively, ρ is the density and $\frac{\Delta I}{I} = (\frac{\Delta V_P}{V_P} + \frac{\Delta\rho}{\rho})$, which is the zero offset P-wave reflection coefficient. Equation 2 can be further simplified by ignoring the third term, which can be proven to be very small for low reflection angles ($< 35^o$) and Poisson's ratio between 0.1 and 0.33. This approximation has been widely used in the industry, but a more generalized study of the problem must seek a different solution if long offset data is to be introduced in AVO analysis. We propose to study the solution

presented in the work of Skopintseva et al. (2011). In their work, they recast the reflectivity problem as an optimization problem, comparing the expected amplitude obtained from a theoretical solution to the one measured in the data. With that, the problem becomes a minimization of an objective function based on the L^2 norm of the two data (calculated and observed):

$$F(v)^2 = \sum_{n=1}^{N} [AVO_{obs}(\mathbf{x_n}) - AVO_{theo}(\mathbf{x_n})]^2, \tag{3}$$

where $\mathbf{x_n}$ represents the receiver coordinates and $\mathbf{n}$ is the receiver number. The theoretical component AVO_{theo} is given by:

$$AVO_{theo}(\mathbf{x_n}) = \frac{\|R_{PP}(\theta(\mathbf{x_n}), \mathbf{m})\|}{\frac{1}{N}\sum_{n=1}^{N} \|R_{PP}(\theta(\mathbf{x_n}), \mathbf{m})\|}, \tag{4}$$

where R_{PP} is the plane reflective coefficient, obtained according to Aizenberg et al. (2005).

To test the validity of this methodology, the first step is to create a synthetic dataset to represent the observed AVO term. We begin by implementing a numerical solution of the elastic wave equation.

Finite difference elastic wave equation

The standard solution to elastic modeling uses the velocity-stress formulation in a staggered-grid approach (Virieux, 1986). The velocities and stresses are the state variables and are evaluated at alternating points in a regularly-sampled grid representation of the property model. The time derivatives of the state variables are also evaluated at alternating time steps. Figure 2 shows schematically where the different properties are evaluated for a single time step.

This staggered grid representation gives good results for finite-difference solutions to the elastic wave equation. Ikelle and Amundsen (2005) show a very comprehensive implementation of a 4^{th} order in time and 2^{nd} order in space staggered-grid finite-difference modeling. The finite-difference representation for the particle velocity component in the x-direction for a 10^{th} order in space and 2^{nd} order in time

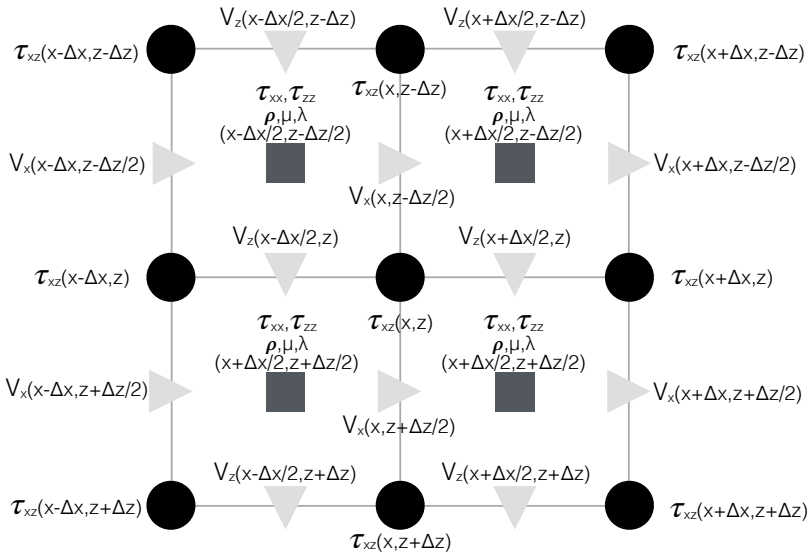

Figure 2: The staggered grid for 2D elastic finite-difference modeling. V_x and V_z represent the particle velocities in the x- and z-directions, respectively, while τ_{xx}, τ_{zz} and τ_{xz} represent the normal and shear stress fields. [**NR**]

operator is:

$$
\begin{aligned}
V_x(x, z+\frac{\Delta z}{2}, t+\frac{\Delta t}{2}) &= V_x(x, z+\frac{\Delta z}{2}, t-\frac{\Delta t}{2}) \\
&+ \frac{\Delta t}{\Delta x} \times (\frac{1}{2}(\frac{1}{\rho(x+\Delta x, z)} + \frac{1}{\rho(x,z)})) \\
&\times (c_1(\tau_{xx}(x+2\Delta x, z+\frac{\Delta z}{2}, t) - \tau_{xx}(x-\frac{5\Delta x}{2}, z+\frac{\Delta z}{2}, t)) \\
&+ c_2(\tau_{xx}(x+\frac{3\Delta x}{2}, z+\frac{\Delta z}{2}, t) - \tau_{xx}(x-2\Delta x, z+\frac{\Delta z}{2}, t)) \\
&+ c_3(\tau_{xx}(x+\Delta x, z+\frac{\Delta z}{2}, t) - \tau_{xx}(x-\frac{3\Delta x}{2}, z+\frac{\Delta z}{2}, t)) \\
&+ c_4(\tau_{xx}(x+\frac{\Delta x}{2}, z+\frac{\Delta z}{2}, t) - \tau_{xx}(x-\Delta x, z+\frac{\Delta z}{2}, t)) \\
&+ c_5(\tau_{xx}(x, z+\frac{\Delta z}{2}, t) - \tau_{xx}(x-\frac{\Delta x}{2}, z+\frac{\Delta z}{2}, t)) \\
&+ \tau_{xx}(x, z+\frac{\Delta z}{2}, t)) \\
&+ (c_1(\tau_{xz}(x, z+\frac{5\Delta z}{2}, t) - \tau_{xz}(x, z-2\Delta z, t)) \\
&+ c_2(\tau_{xz}(x, z+2\Delta z, t) - \tau_{xz}(x, z-\frac{3\Delta z}{2}, t)) \\
&+ c_3(\tau_{xz}(x, z+\frac{3\Delta z}{2}, t) - \tau_{xz}(x, z-\Delta z, t)) \\
&+ c_4(\tau_{xz}(x, z+\Delta z, t) - \tau_{xz}(x, z-\frac{\Delta z}{2}, t)) \\
&+ c_5(\tau_{xz}(x, z+\frac{\Delta z}{2}, t) - \tau_{xz}(x, z, t)))
\end{aligned}
\tag{5}
$$

where V_x is the particle velocity in the x direction; $\rho(x,z)$ is the density at location (x,z); $\tau_{xx}(x,z,t)$ is the normal stress component in the x direction; $\tau_{xz}(x,z,t)$ is the shear stress at location (x,z) and time t; and c_1 to c_5 are the finite-difference coefficients, according to (Liu and Sen, 2009).

The z-component of the particle velocity field and the three stress components can be obtained in a similar way to equation 5. However, it is important to note that different properties are evaluated at different grid points according to Figure 2. This means that care must be taken when defining the derivatives, in order to preserve the symmetry of the central difference operator.

The reason to apply such a high-order approximation to the numerical modeling is to minimize dispersion error for large simulation times without the need for very fine modeling grids. Since we are interested in the amplitudes, it is essential that the wavelet is not affected by numerical artifacts and behaves accordingly to the physical equations. As an example of such dispersive effects, we refer to the work of Souza et al. (2013), who compares the traditional 4^{th} order stencil to a 12^{th} order one and their respective numerical dispersions.

RESULTS

We show results of applying our modeling algorithm to a constant velocity model, a constant model with a flat reflector and a model with increasing velocity with depth and a horizontal reflector. These simple modeling runs are aimed at testing the stability of the numerical propagation, the mode conversions between P waves and S waves and finally the presence of turning waves on the last example.

The first example was modeled for a constant property model with an explosive source at its center. The source is a Ricker wavelet with a peak frequency of 25 Hz. The resulting elastic wavefront can be seen in Figures 3(a) and 3(b), which show the particle displacement in the x-direction and z-direction for t = 350 ms, respectively.

For the second example, we added a reflector at a depth of 1500 m below the source and extended the model laterally to 20 km (see Figure 4). Figure 5(a) shows a snapshot for the wavefield's particle velocity in the x direction for a source place at x = 600 m and z = 500 m. We calculated the divergence and curl of the particle velocities. For an isotropic wavefield, these operations separate the P and S waves. Figures 6(a) and 6(b) show the P-wave and S-wave seismograms, respectively.

The final example (see Figure 7) has a background velocity that linearly increases with depth in addition to the horizontal reflector from the previous example. The goal here is to show the appearence of turning waves in the modeling, as we can see in Figures 8(a), 8(b), 9(a) and 9(b). These show snapshots of the particle displacement in the x-direction, z-direction and the corresponding P and S seismograms, respectively.

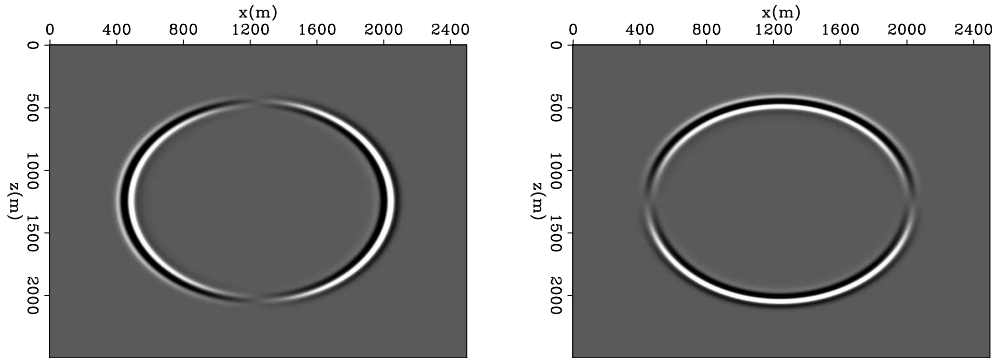

Figure 3: Snapshot of the particle displacement in (a) the x-direction and (b) the z-direction for time t = 350 ms. The source is explosive, with a Ricker wavelet of peak frequency of 25Hz. [**ER**]

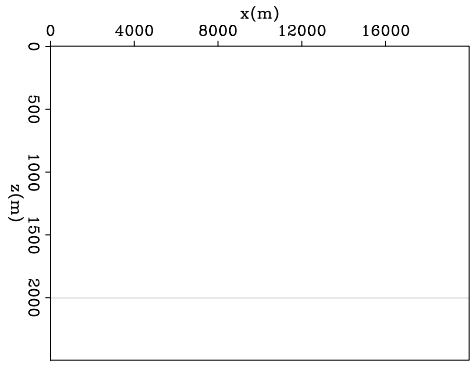

Figure 4: P velocity model for the constant background velocity model with a reflector at z = 2000 m. The background P velocity is equal to 2700 m/s, with a density of $\rho = 2750$ kg/m^3. The reflector has a P velocity of 1500 m/s and density of $\rho = 1000$ kg/m^3. S velocities are calculated as half of the P velocities. The boundary conditions are included in this image, so the source for this model is located at x = 600 m and z = 500 m. [**ER**]

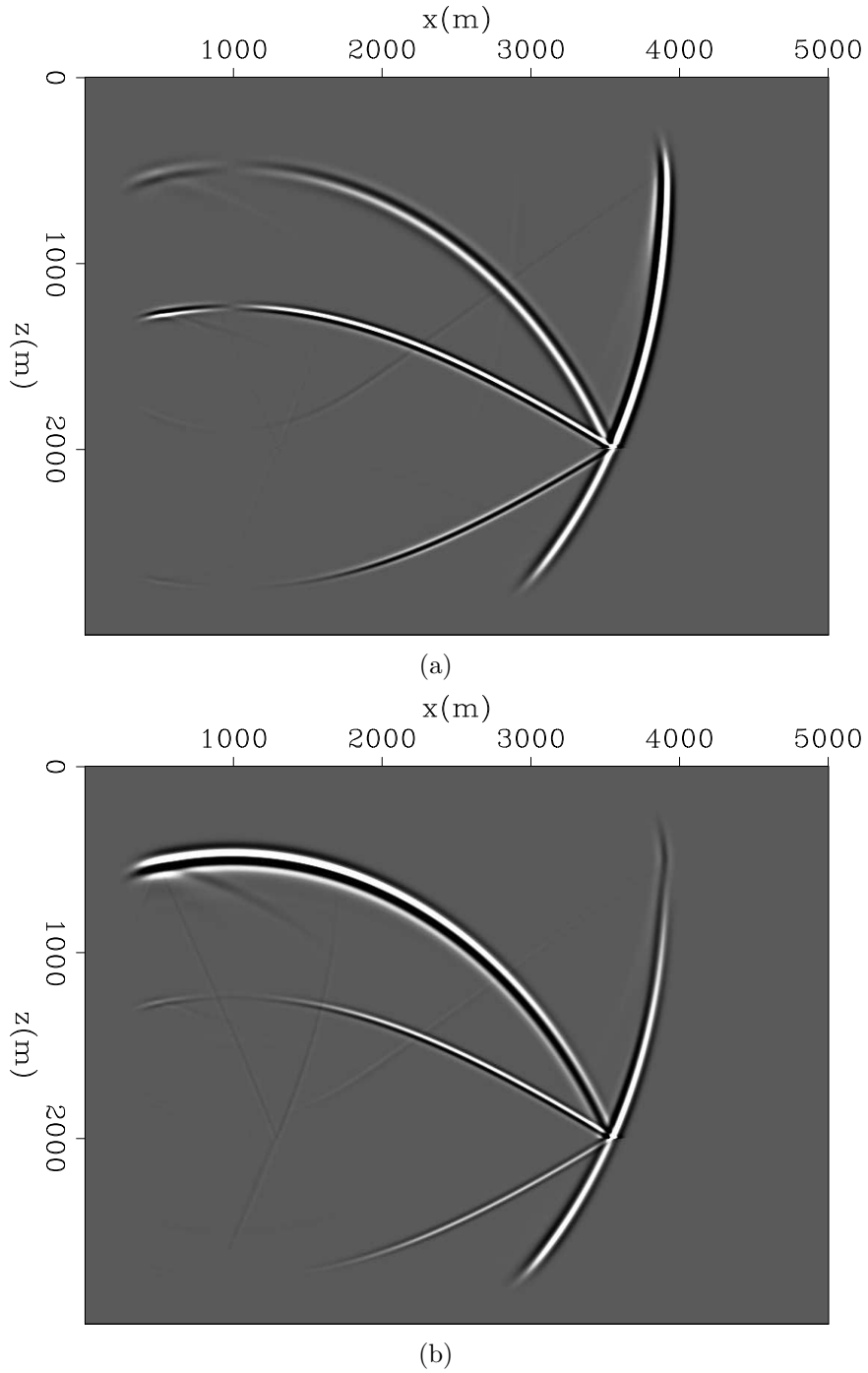

Figure 5: Snapshot for time t = 1.2 s for (a) the x-component and (b) the z-component of the particle velocity in a constant background model with one horizontal reflector. [**ER**]

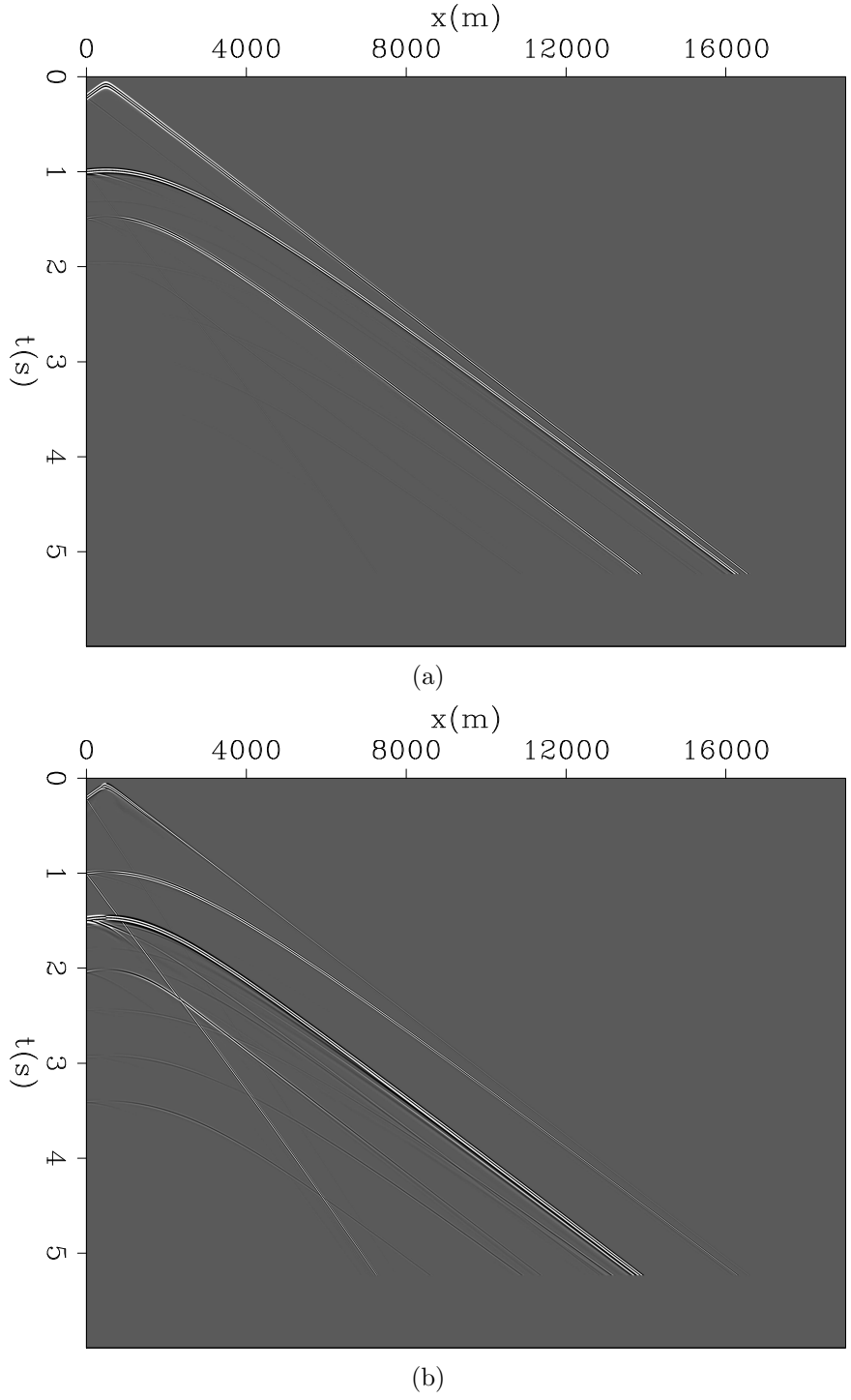

Figure 6: (a) P seismogram obtained from the divergent of the particle velocities for a constant background with a single horizontal reflector; (b) S seismogram obtained from the curl of the particle velocities for the same model. [**ER**]

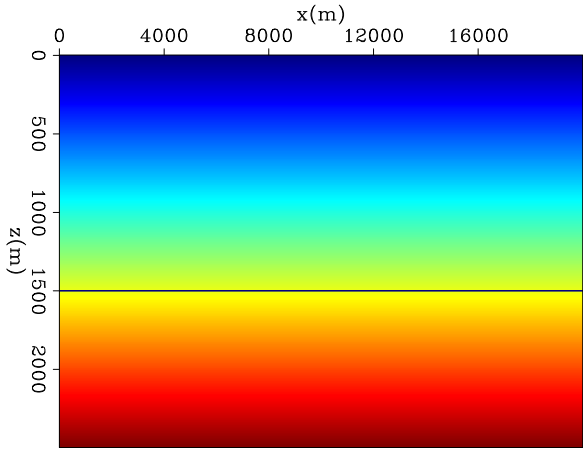

Figure 7: P velocity model for a depth increasing V(z) with a horizontal reflector at z = 2000 m. The values for the reflector and background properties are the same as in Figure 4, but here the background P and S velocities linearly increase to 4200 m/s and 2100 m/s, respectively. [**ER**]

DISCUSSION

The literature shows many possible studies related to long-offset data. The estimation of better velocity models holds great interest for applications in FWI, such as the aforementioned examples. Also, research related to amplitude analysis appears to be a promising area of study, with interesting examples that may extend AVO analysis to longer offset data.

The results shown in this work are a preliminary effort in the direction of amplitude analysis. Future work will be aimed at applying this modeling methodology to study long-offset amplitudes and possible ways to efficiently evaluate them in field data.

Finally, this approach is aimed at 2D modeling. A 3D solution to this same problem will involve complications that have not yet been addressed in this work.

ACKNOWLEDGMENT

The authors would like to thank the Stanford Exploration Project sponsors for the ongoing support. Gustavo would like to thank Petrobras for support of his PhD.

REFERENCES

Aizenberg, A., M. Ayzenberg, H. Helle, and J. Pajchel, 2005, Reflection and transmission of acoustic wavefields at a curved interface of two inhomogeneous media: Continuum Dynamics: Acoustics of Inhomogeneous Media, **123**, 73–79.

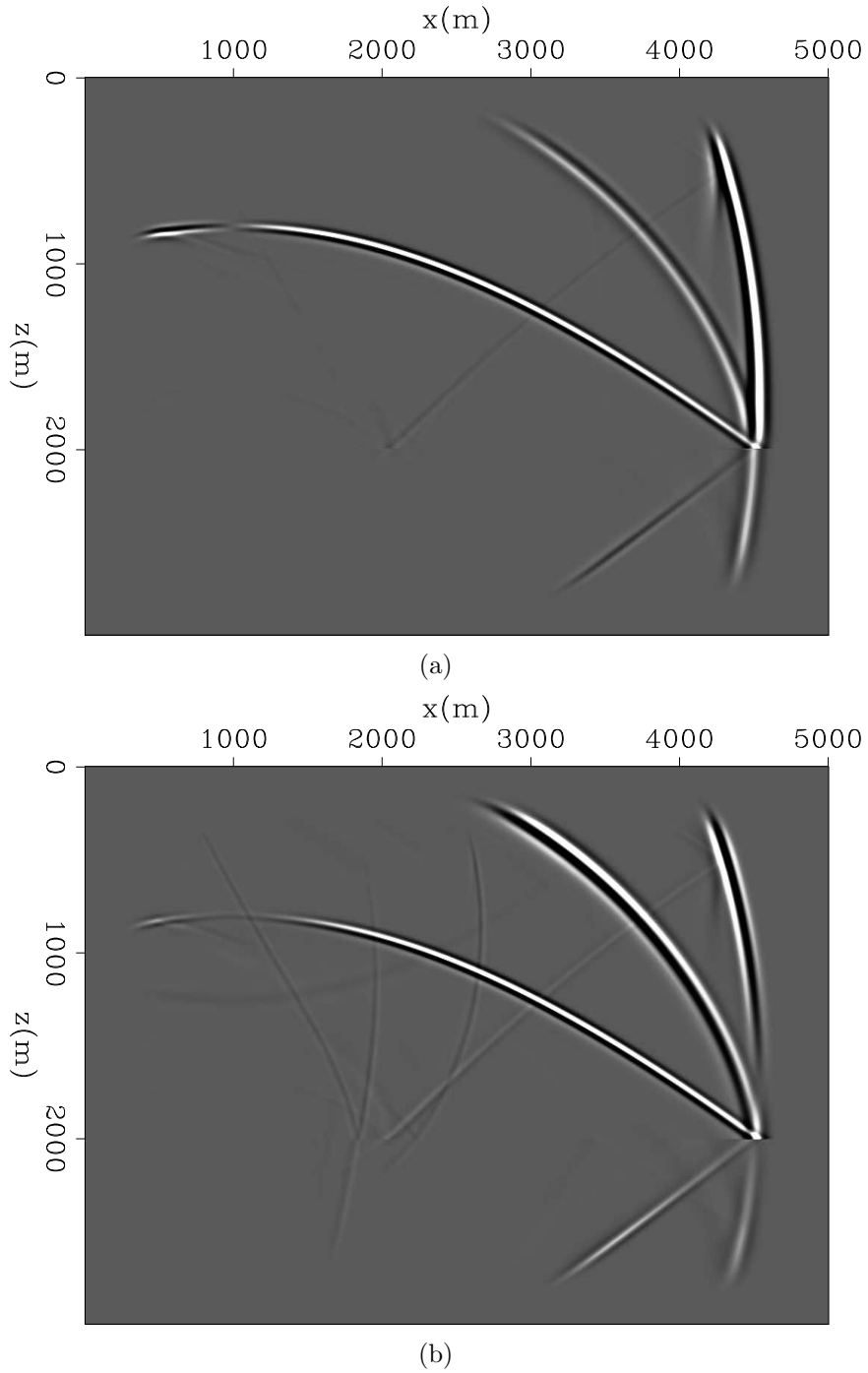

Figure 8: Snapshot for time t = 1.2 s for (a) the x-component and (b) the z-component of the particle velocity in a V(z) model with one horizontal reflector. [**ER**]

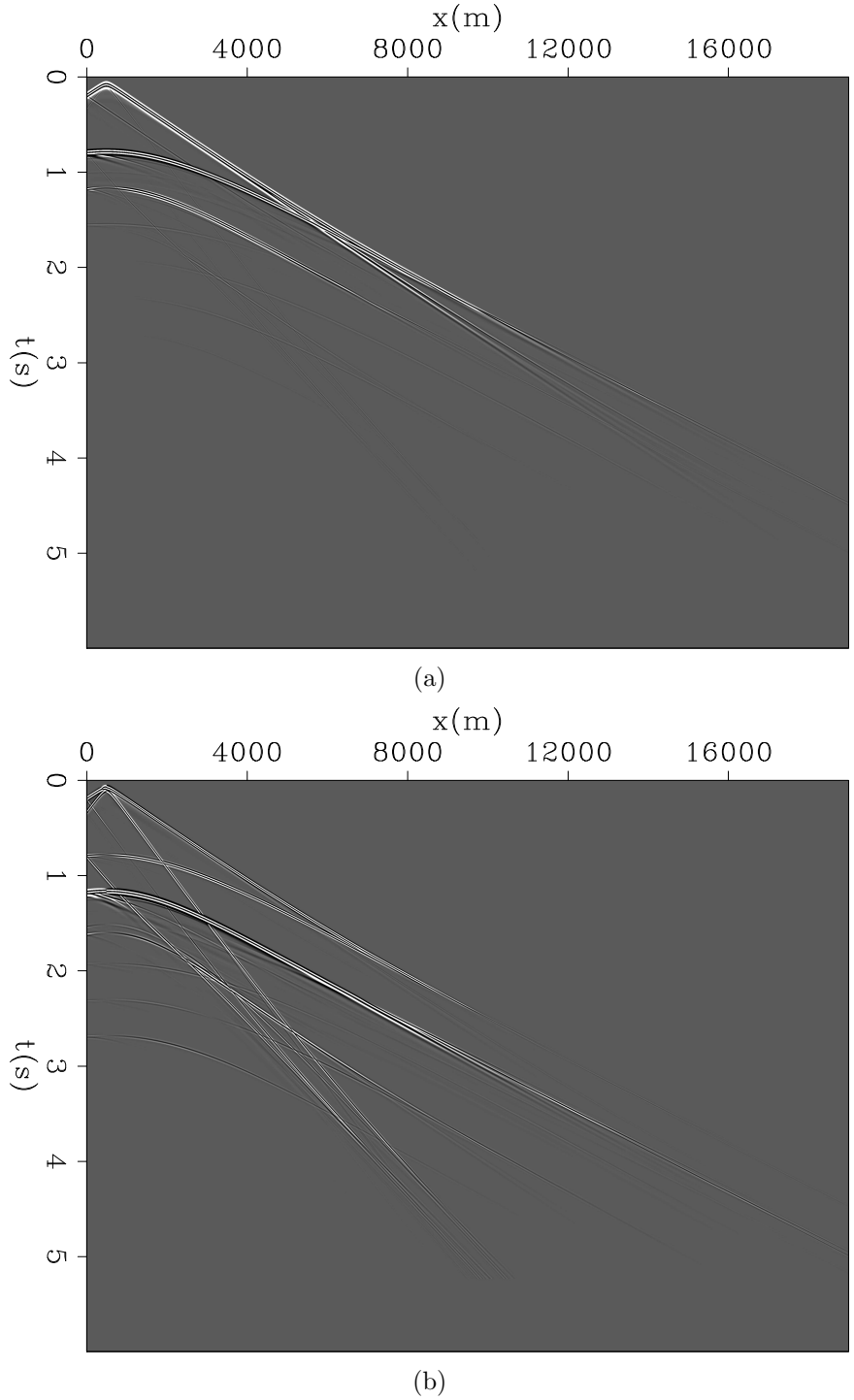

Figure 9: (a) P seismogram obtained from the divergent of the particle velocities for a V(z) background with a single horizontal reflector; (b) S seismogram obtained from the curl of the particle velocities for the same model. [**ER**]

Aki, K. and P. G. Richards, 1980, Quantitative seismology: Theory and methods, 1: I: WH Freeman and Co.

Brenders, A., R. G. Pratt, et al., 2007, Waveform tomography of marine seismic data: What can limited offset offer: 75th Annual International Meeting, SEG, Expanded Abstracts, 3024–3029.

Corcoran, C., C. Perkins, D. Lee, P. Cattermole, R. Cook, and N. Moldoveanu, 2007, A wide-azimuth streamer acquisition pilot project in the Gulf of Mexico: The Leading Edge, **26**, 460–468.

Fatti, J. L., G. C. Smith, P. J. Vail, P. J. Strauss, and P. R. Levitt, 1994, Detection of gas in sandstone reservoirs using AVO analysis: A 3-D seismic case history using the Geostack technique: Geophysics, **59**, 1362–1376.

Hilterman, F., C. Van Schuyver, and M. Sbar, 2000, AVO examples of long-offset 2-D data in the Gulf of Mexico: The Leading Edge, **19**, 1200–1213.

Ikelle, L. and L. Amundsen, 2005, Introduction to petroleum seismology: Society of Exploration Geophysicists Tulsa, OK.

Liu, Y. and M. K. Sen, 2009, An implicit staggered-grid finite-difference method for seismic modelling: Geophysical Journal International, **179**, 459–474.

Moldoveanu, N., J. Kapoor, and M. Egan, 2008, Full-azimuth imaging using circular geometry acquisition: The Leading Edge, **27**, 908–913.

Skopintseva, L., M. Ayzenberg, M. Landrø, T. Nefedkina, and A. M. Aizenberg, 2011, Long-offset AVO inversion of PP reflections from plane interfaces using effective reflection coefficients: Geophysics, **76**, C65–C79.

Souza, A. A., A. Bulcão, B. P. Dias, D. M. S. Filho, F. P. Loureiro, F. F. Farias, G. C. Alves, L. A. Santos, and R. F. da Cruz, 2013, Anti-dispersive acoustic seismic modeling: Presented at the 2013 Congress of the Brazilian Geophysics Society.

Virieux, J., 1986, P-SV wave propagation in heterogeneous media: Velocity-stress finite-difference method: Geophysics, **51**, 889–901.

Zadeh, H. M., M. Landrø, and O. I. Barkved, 2010, 4D Critical Angle Analysis Using Valhall LoFS Data: 2010 SEG Annual Meeting, 4145–4149.